Ag[B(S2O7)2]: the first transition metal borosulfate featuring disulfate groups

Philip Netzsch, Henning A. Höppe

Angaben zur Veröffentlichung / Publication details:

Netzsch, Philip, and Henning A. Höppe. 2021. "Ag[B(S2O7)2]: the first transition metal borosulfate featuring disulfate groups." *European Journal of Inorganic Chemistry* 11: 1065–70. https://doi.org/10.1002/ejic.202001095.

EurJIC
European Journal of Inorganic Chemistry

Full Papers
doi.org/10.1002/ejic.202001095

Chemistry Europe
European Chemical Societies Publishing

$Ag[B(S_2O_7)_2]$: The First Transition Metal Borosulfate Featuring Disulfate Groups

Philip Netzsch[a] and Henning A. Höppe*[a]

Dedicated to Prof. Christoph Janiak on the occasion of his 60th birthday.

Hitherto, the structural diversity of transition metal borosulfates has been limited to B–O–S and B–O–B bridges. $Ag[B(S_2O_7)_2]$ represents the very first transition metal borosulfate featuring S–O–S bridges. The compound was synthesized solvothermally in oleum (65 % SO_3) and crystallizes in a new structure type in $P2_1/c$ (no. 14) with $Z=4$, $a=950.7(4)$ pm, $b=960.1(4)$ pm, $c=1173.0(4)$ pm and $\beta=98.350(11)°$. The crystal structure comprises complex anions $[B(S_2O_7)_2]^-$ – consisting of a central boron atom and two chelating disulfate groups – and charge balancing Ag^+ ions. Vibrational spectroscopy confirms the presence of S–O–S bridges. A thermal decomposition from $Ag[B(S_2O_7)_2]$ towards $Ag[B(SO_4)_2]$ was monitored by means of thermogravimetric analysis (TGA) and temperature programmed X-ray diffraction (TPXRD).

Introduction

Borosulfates are silicate-analogous materials consisting of corner-sharing borate and sulfate tetrahedra.[1] Starting from the first borosulfate $K_5[B(SO_4)_4]$ eight years ago[2] ongoing research led to enormous progress in borosulfate chemistry. Besides the structural evolution, especially optical properties were investigated showing a weak coordination behavior of the borosulfate anions[3–5] or even second harmonic generation responses.[6] A striking prospect for borosulfate chemistry, however, could be as electrolytes for solid acid fuel cells, since a high proton conductivity for the ammonium borosulfates $NH_4[B(SO_4)_2]$ was reported, recently.[7] Next to proton conductivity, theoretical calculations on solid state Li-ion conductors revealed $Li_5[B(SO_4)_4]$ as a potential fast-ion conductor.[8] In this context also silver compounds might be highly interesting due to their well-documented frequent ion conductivity.[9–11] In case of borosulfates, only one silver compound $Ag[B(SO_4)_2]$ is known so far, which is homeotypic with the aforementioned $NH_4[B(SO_4)_2]$.[12]

Even though several transition metal borosulfates are reported up to date, there is still a lack of structural diversity within this section of the periodic table. Meanwhile we differentiate between *classic* and *unconventional* borosulfates. In *classic* borosulfates the anions consist solely of alternating borate and sulfate tetrahedra like in $M[B_2(SO_4)_4]$ (M = Mn, Co, Ni, Cu, Zn),[5,13–15] and in the protonated borosulfate $Cu[B(HSO_4)(SO_4)_2]$.[13] In *unconventional* borosulfates the anions may feature B–O–B bridges as reported for $M_4[B_2O(SO_4)_6]$ (M = Mn, Co, Ni, Zn).[3] However, no transition metal borosulfates featuring S–O–S bridges – also classified as *unconventional* – could be synthesized so far. In this context, the *tris*-(disulfato)-metallates $Ag_2[M(S_2O_7)_3]$ (M = Si, Ge, Sn) are worth mentioning, comprising an octahedrally coordinated metal cation M^{4+} by three chelating disulfate groups.[16] Moreover, the silver disulfate $Ag_2S_2O_7$ and the silver pentasulfate $Ag_2[S_5O_{16}]$ are both ternary compounds of condensed sulfate tetrahedra.[17,18]

Recently, we were able to achieve great progress in selective syntheses of borosulfates with respect to their connection pattern.[19,20] Thus, we could report on the first quaternary systems MO–B_2O_3–SO_3 (M = Sr, Ba), where each connection pattern – S–O–S, B–O–S and B–O–B bridges ..– could be synthesized carefully controlling the oleum concentration during the synthesis. Consequently, this should enable the synthesis of novel transition metal borosulfates containing disulfate groups, *i.e.* S–O–S bridges. The most common borosulfate anion with S–O–S bridges is the molecular anion $[B(S_2O_7)_2]^-$ which can be found in the alkali metal and ammonia borosulfates $A[B(S_2O_7)_2]$ (A = Li, Na, K, NH_4)[21–23] and alkaline earth metal borosulfate $Ba[B(S_2O_7)_2]_2$.[19]

Herein, we focus on precious metal borosulfates in particular, as ternary noble metal sulfates or disulfates often show a fascinating crystal chemistry and interesting properties. In $AuSO_4$, for example, the structure features Au_2^{4+} dumbbells,[24] in $Pd(S_2O_7)$ octahedrally coordinated Pd^{2+} ions and ferromagnetic ordering were observed[25] and in $AgSO_4$ strong one-dimensional antiferromagnetic interactions of Ag^{2+} ions were reported.[26]

In our contribution we present $Ag[B(S_2O_7)_2]$ – the first transition metal borosulfate featuring S–O–S bridges. We elucidate the crystal structure and characterize the compound by X-ray powder diffraction, vibrational spectroscopy, thermogravimetric analysis and temperature programmed X-ray diffraction.

[a] P. Netzsch, Prof. Dr. H. A. Höppe
Lehrstuhl für Festkörperchemie
Universität Augsburg
Universitätsstr. 1, 86159 Augsburg
E-mail: henning@ak-hoeppe.de
https://www.ak-hoeppe.de

Supporting information for this article is available on the WWW under https://doi.org/10.1002/ejic.202001095

Results and Discussion

Crystal Structures

$Ag[B(S_2O_7)_2]$ crystallizes in a new structure type in space group $P2_1/c$ (no. 14) with four formula units per unit cell (Figure 1). The structure is built by the complex anion $[B(S_2O_7)_2]^-$ of a boron atom and two chelating disulfate groups (Figure 2). Thus, two six-membered rings (BS_2O_3) result, both in the chair conformation. This is similar to the anion in $Ba[B(S_2O_7)_2]_2$, whereas in $A[B(S_2O_7)_2]$ (A = Li, Na, K, NH_4) at least one ring is in a twisted conformation (Figure S3). In general, such huge anions carrying only one negative charge are a crystal-chemistry problem – as cations require a certain coordination number – and will thus strive for a spherical shape as possible. Due to the presence of these bridged sulfate tetrahedra, this moiety violates *Pauling*'s fourth rule, which states that in a crystal comprising tetrahedra of differently charged cations, those with high valence avoid condensation.[27] This can be realized by the usage of pure oleum (65 % SO_3) during the synthesis. Consequently, a high tendency towards condensation results, as observed in several oligosulfates.[28] Two disulfate groups thus coordinate the central boron atom in order to minimize the anions surface, comparable to the anion $[Si(S_2O_7)_3]^{2-}$ in $Ag_2[Si(S_2O_7)_3]$.[16] The central borate tetrahedron shows B–O bond lengths between 145.5(3)–149.2(2) pm and can be classified as regular due to a deviation of −0.35 % from the tetrahedral symmetry.[29,30] Within the sulfate tetrahedra, three different bond length regimes can be discerned, in line with three different bonding situations (Table 1). Short S-O^t bond lengths are found for the terminal oxygen atoms, ranging from 140.80(17) to 142.72(15) pm. For the bridging oxygen atom towards the borate tetrahedron, longer S–O^{br} bond lengths are found between 152.18(15) and 153.67(15) pm. Due to the strong repulsion between the high valent sulfur atoms, the S–O^S bond lengths of 161.41(15) to 163.55(15) pm for the bridging oxygen atom within the disulfate group are significantly longer. Despite this elongated bond length, the deviation from the tetrahedral symmetry amounts between −0.14 and −0.18 % for all sulfate tetrahedra. The bond lengths are in good agreement with data reported for similar borosulfate anions.[19,21] Each anion coordinates six silver cations by terminal oxygen atoms stemming from the sulfate tetrahedra. Therein, one silver cation is coordinated bidentately. In comparison to other borosulfates featuring the $[B(S_2O_7)_2]^-$ anion, such a chelating ligand is only observed for the larger cations like Ba^{2+} and K^+, whereas the smaller ones like Li^+ and Na^+ are solely coordinated monodentately. Two terminal oxygen atoms remain uncoordinated resulting in slightly higher atomic displacement parameters for O31 and O41 (Figure 2 and Table S2).

The silver cation itself is coordinated by seven oxygen atoms from five monodentately and one bidentately anion. The coordination environment can be described as distorted monocapped trigonal prism (Figure 3). The average Ag–O distances

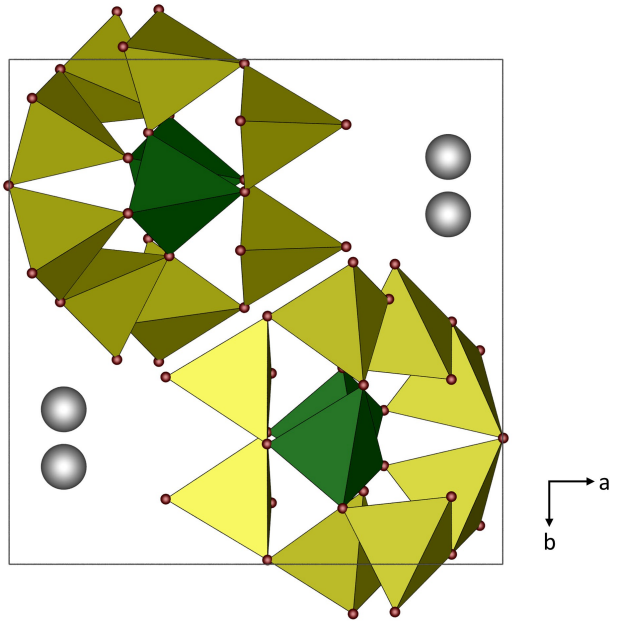

Figure 1. Crystal structure of $Ag[B(S_2O_7)_2]$ viewed along the *c* direction; borate tetrahedra in green, sulfate tetrahedra in yellow, oxygen atoms as red spheres.

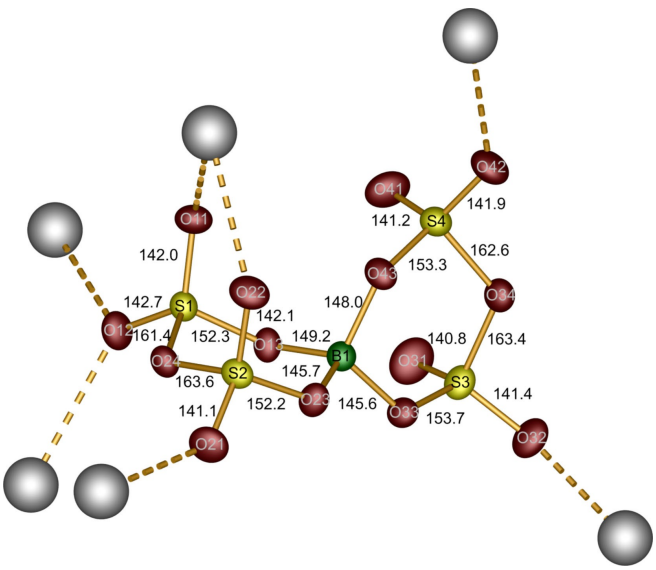

Figure 2. (a) distorted capped trigonal prismatic coordination environment of Ag^+ and (b) extended coordination environment.

Table 1. Selected interatomic distances (in pm) and angles (in °) in $Ag[B(S_2O_7)_2]$ (esds in parentheses).

	$Ag[B(S_2O_7)_2]$
Ag–O	247.33(17)–277.17(19)
Σr_{ion}(Ag–O)	257
S–O^t	140.07(15)–142.11(14)
S–O^b	151.79(13)–153.00(14)
S–O^s	160.89(14)–164.75(13)
B–O	145.5(2)–148.5(2)
O–S–O	99.74(7)–119.87(10)
O–B–O	105.13(14)–111.92(13)

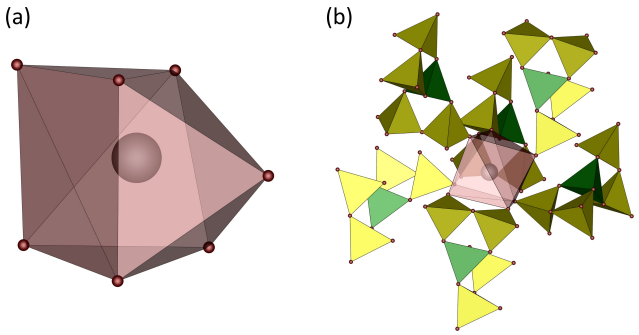

Figure 3. $[B(S_2O_7)_2]^-$ anion with the corresponding atom labelling, bond distances and coordinated silver cations; thermal ellipsoids are set to 70% probability.

of 258.8 pm correspond very well with the sum of the ionic radii of 257 pm.[31] Therein, each oxygen atom coordinates only one silver cation, leading to highly separated silver cations with Ag–Ag distances of 438.49(14) pm. This value is even above the one reported for $Ag[B(SO_4)_2]$.[12] Consequently, the d^{10}-d^{10} interactions frequently found in silver compounds are not observed here, since the Ag–Ag distances are far beyond the typical distances for such phenomena.[32]

The coordination number of seven for silver as well as the electrostatic consistency of the new crystal structure is confirmed by calculations based on the MAPLE (*MA*delung *P*art of the *L*attice *E*nergy) concept (Tables S3–S4).[33–35]

Vibrational spectroscopy

The FT-IR spectrum is depicted in Figure 4 (full spectrum in Figure S4) and shows bands between 1500–400 cm^{-1}, which is the typical region for borate and sulfate tetrahedra.[36] The spectrum is in good agreement with the one recently reported for $Ba[B(S_2O_7)_2]_2$ comprising the topological same $[B(S_2O_7)_2]^-$ anion.[19] Therein, we calculated the spectrum based on density functional theory, which enables an assignment of the bands in $Ag[B(S_2O_7)_2]$ as well (Table 2).

The asymmetric stretching vibration $\nu_{asym}(S–O_{nc.})$ involving the non-coordinated oxygen atoms occurs at 1413 cm^{-1}, whereas the ones involving coordinated oxygen atoms occur at 1373 and 1213 cm^{-1}. At 1196 and 1169 cm^{-1} the symmetric stretching vibrations $\nu_{sym}(S–O)$ can be found. The symmetric stretching vibrations within the borate tetrahedron can be assigned to the bands at 1043 and 984 cm^{-1}. At 947 cm^{-1} asymmetric stretching vibrations in the borate and sulfate tetrahedra are monitored. Bending vibrations $\delta(O–B-O)$ can be found at 925 and 892 cm^{-1}. The bands at 794, 784, 730 and 705 cm^{-1} can be assigned to stretching vibrations $\nu(S–O_b)$ involving the bridging oxygen atom in the disulfate group. This proves the presence of these disulfate groups, since calculations on $Ag[B(SO_4)_2]$ show no bands in the region between 800 and 700 cm^{-1}.[12] Below 650 cm^{-1}, the spectrum is dominated by bending vibrations of the sulfate and borate tetrahedra.

Thermal analysis

In case of main group metal borosulfates, compounds featuring S–O–S bridges typically decompose towards further borosulfates featuring solely B–O–S bridges.[19–21] Consequently, we investigated the thermal behavior of $Ag[B(S_2O_7)_2]$ as an example of the first transition metal borosulfate with disulfate groups.

Indeed, the thermogravimetric analysis (Figure 5) shows two decomposition steps. The first one is addressed to the transformation of $Ag[B(S_2O_7)_2]$ to $Ag[B(SO_4)_2]$, by the release of two moles SO_3 per complex anion originating from the respective two disulfate groups ($\Delta m_{calc.} = 34.0$ wt%):

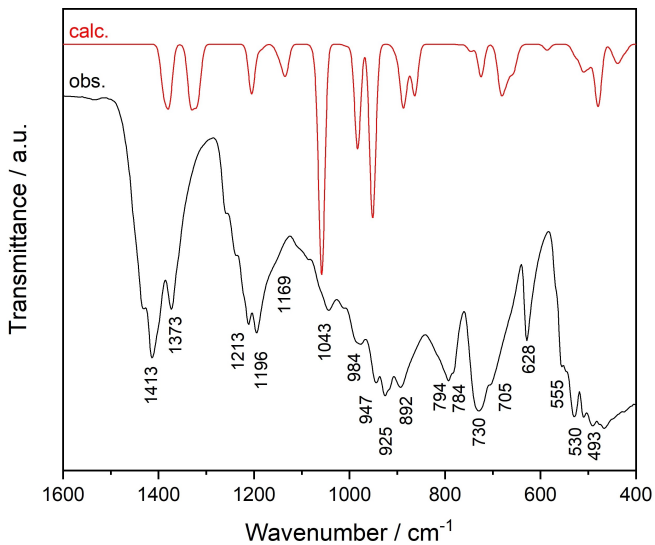

Figure 4. Observed FT-IR spectrum of $Ag[B(S_2O_7)_2]$ (black) and the calculated spectrum of $Ba[B(S_2O_7)_2]_2$ (red).

Table 2. IR vibrational modes in $Ag[B(S_2O_7)_2]$ in comparison to the calculated spectrum of $Ba[B(S_2O_7)_2]_2$ and their assignments.[a]

IR exp. [Freq./cm^{-1}]		IR calc. [Freq./cm^{-1}]	Assignment
1413	s	1388/1377	$\nu_{asym}(S–O_{nc.})$
1373	s	1333/1322/1316	$\nu_{asym}(S–O)$
1213	s	1204	$\nu_{asym}(S–O)$
1196	s	1143	$\nu_{sym}(S–O)$
1169	s	1133	$\nu_{sym}(S–O)$
1043	m	1058	$\nu_{sym}(B–O)$
984	m	983	$\nu_{sym}(B–O)$
947	m	951/949	$\nu_{asym}(B–O)$, $\nu_{asym}(S–O)$
925	m	902	$\delta(O–B-O)$
892	m	888/863	$\delta(O–B-O)$
794	s	745	$\nu(S–O_b)$
784	sh	725/724	$\nu(S–O_b)$
730	s	682	$\nu(S–O_b)$
705	sh	670/657	$\nu(S–O_b)$
628	s	586	$\delta(O–S-O)$
555	sh	511	$\delta(O–S-O)$
530	s	481	$\delta(O–B–O)$, $\delta(O–S–O)$
493	m	446	$\delta(O–B–O)$, $\delta(O–S–O)$

[a] s = strong, m = medium, w = weak, sh = shoulder.

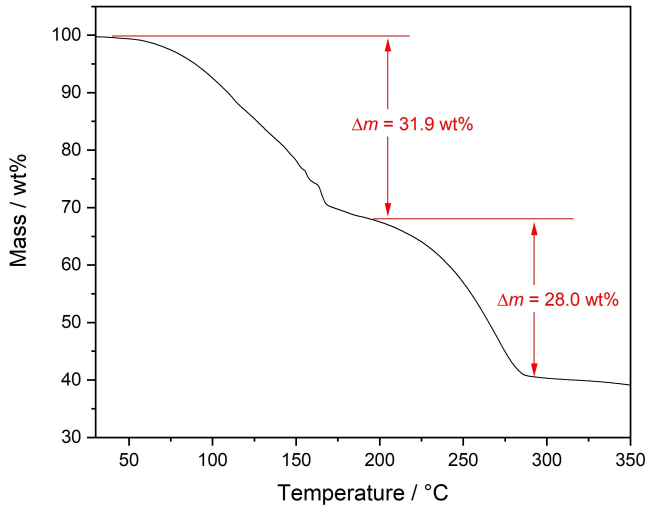

Figure 5. Thermogravimetric analysis of $Ag[B(S_2O_7)_2]$, recorded under nitrogen atmosphere with a heating ramp of 10 °C/min.

$$Ag[B(S_2O_7)_2] \rightarrow Ag[B(SO_4)_2] + 2\ SO_3$$

The transformation can be described similarly to $Ba[B(S_2O_7)_2]_2$ as a condensation of the complex anions $[B(S_2O_7)_2]^-$ to one-dimensional chains $_\infty^1[B(SO_4)_2]^-$ along the *c* direction of the respective crystal structures (Figure 6).[19] In the second step, the borosulfate anion decomposes to form silver sulfate Ag_2SO_4 and amorphous B_2O_3 ($\Delta m_{calc.} = 25.5$ wt%), as confirmed by PXRD of the residue from the TGA (Figure S5):

$$Ag[B(SO_4)_2] \rightarrow 0.5\ Ag_2SO_4 + 0.5\ B_2O_3 + 1.5\ SO_3$$

The observed mass losses of 31.9 and 28.0 wt%, respectively, deviate slightly from the observed ones. This can be explained by a partial overlap of the two decomposition steps, as the overall mass loss of 59.9 wt% matches very well with the calculated one of 59.5 wt%. In order to confirm the above-mentioned decomposition reactions, temperature programmed X-ray diffraction (TPXRD) was employed as *in situ* method. Therein, the transformation of $Ag[B(S_2O_7)_2]$ to $Ag[B(SO_4)_2]$ is clearly visible by the powder patterns above $T = 150$ °C (Figure 7).

Unlike the decompositions of the divalent metal borosulfates $Ba[B(S_2O_7)_2]_2$ and $Sr[B_2(SO_4)_3(S_2O_7)]$,[19,20] no further transformation from B–O–S bridges towards B–O–B bridges was observed. Similarly, for the monovalent metal and non-metal borosulfates $A[B(S_2O_7)_2]$ (A = Li–K, NH_4) also only a transformation from S–O–S bridges to B–O–S bridges was reported, so that the corresponding borosulfates with B–O–B bridges remained unknown so far.[21,22] Interestingly, this structural feature could only be observed for the larger alkali metals rubidium and cesium in $Rb_4[B_2O(SO_4)_4]$ and $Cs_2[B_2O(SO_4)_3]$, respectively.[23] Presumably, for the smaller monovalent cations such as Ag^+, B–O–B bridges are obviously less stabilized leading directly to the respective sulfate.

Conclusion

Herein, we presented the first access to transition metal borosulfates featuring S–O–S bridges. By using 65% SO_3 containing oleum under solvothermal conditions, $Ag[B(S_2O_7)_2]$ was obtained as a phase pure crystalline powder. Thus, the higher SO_3 content with respect to the oleum (20% SO_3) used for the synthesis of $Ag[B(SO_4)_2]$ enabled the formation of disulfate groups within the borosulfate anion. These consist of a central boron atom, which is tetrahedrally coordinated by two chelating disulfate groups leading to the complex anion $[B(S_2O_7)_2]^-$. Charge compensation is achieved by monovalent silver cations.

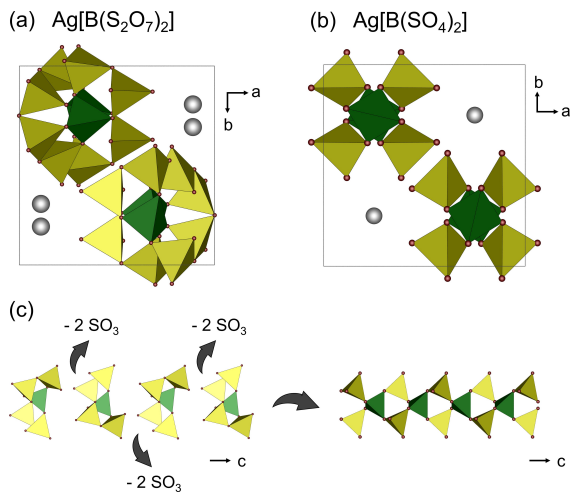

Figure 6. Crystal structures of (a) $Ag[B(S_2O_7)_2]$ and (b) $Ag[B(SO_4)_2]$ viewed along *c* direction; (c) schematic process of the condensation of the $[B(S_2O_7)_2]^-$ complex anions towards $[B(SO_4)_2]^-$ anionic chains.

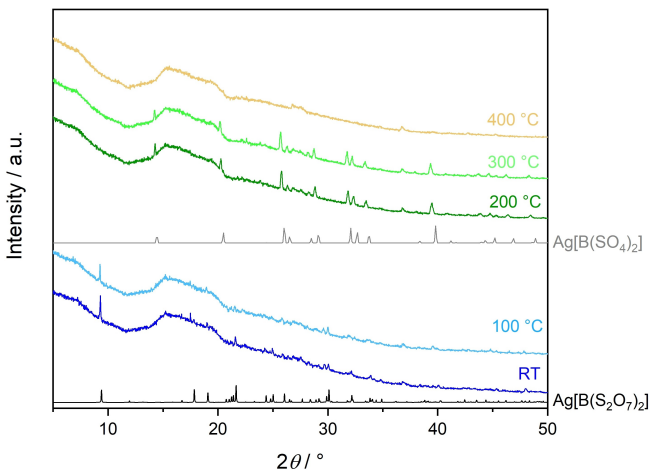

Figure 7. Comparison of TPXRD patterns of initial $Ag[B(S_2O_7)_2]$ from room temperature to 400 °C (RT: dark blue, 100 °C: blue, 200 °C: dark green, 300 °C: green, 400 °C: brown) with calculated patterns of $Ag[B(S_2O_7)_2]$ (black) and $Ag[B(SO_4)_2]$ (gray).

We could show that these complex anions condense upon heating to one-dimensional chains according to $_{\infty}^{1}[B(SO_4)_2]^-$ in the above-mentioned $Ag[B(SO_4)_2]$ by the release of SO_3 originating from the disulfate groups.

In a nutshell, the achieved progress concerning the structural diversity of outer transition metal borosulfates should be transferable to the inner transition metals as well, where so far only one crystal structure type, namely $Ln_2[B_2(SO_4)_6]$ (Ln = La–Lu), is known, which features solely B–O–S bridges. Respective investigations are currently underway in our laboratories.

Experimental Section

Synthesis

$Ag[B(S_2O_7)_2]$ was synthesized by loading Ag_2CO_3 (0.5 mmol, 0.0738 g) and B_2O_3 (1 mmol, 0.0696 g) into a silica ampule (length: 21 cm, diameter: 1 cm, wall thickness: 0.1 cm) followed by the addition of 1 ml oleum (65 % SO_3). The length of the ampule plays a decisive role, since no crystallization has taken place in ampules shorter than 21 cm.

The ampule was torch-sealed, and the following temperature program was applied: heating to 180 °C with 12.5 °C/h, holding the temperature for 12 h and cooling down to room temperature with 6 °C/h (**Caution**: During and even after the reaction, the ampules are under remarkable pressure and must therefore be handled with great care, e.g., they must be cooled with liquid nitrogen before opening).

Colorless, single crystal needles of $Ag[B(S_2O_7)_2]$ were formed in the acid (Figures S1 and S2) and the yield was quantitative with respect to the initial Ag_2CO_3. After opening, the crystals were transferred and stored in an argon filled glovebox. The phase purity was confirmed by a Rietveld refinement on the PXRD data (Figure 8).

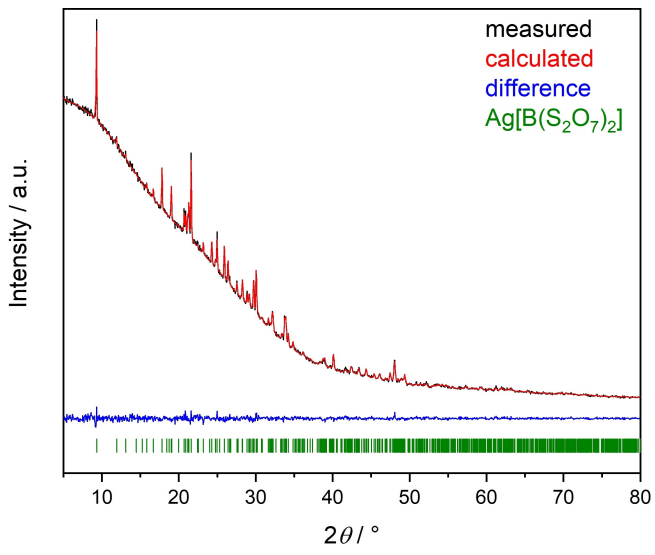

Figure 8. Rietveld refinement of $Ag[B(S_2O_7)_2]$; measured (black line) and calculated (red line) powder diffraction pattern; calculated reflection positions (green vertical bars) and the difference plot (blue line).

Crystal structure determination

Immediately after opening the ampule, single-crystals were transferred into perfluorinated polyether and selected for single-crystal XRD. Diffraction data were collected with a Bruker D8 Venture diffractometer using Mo-K_α radiation (λ = 0.71073 Å). The temperature was adjusted with a nitrogen flow (Oxford Cryosystems). The absorption correction was performed employing the multi-scan method;[37] then the crystal structure was solved with direct methods within the SHELXS program[38] and refined by the full-matrix least-squares technique within the SHELXTL program.[39]

Further details of the crystal structure investigation discussed in this contribution are listed in Table 3 as well as Table S1 and Table S2 in the supporting information.

Deposition Number 2048175 (for $Ag[B(S_2O_7)_2]$) contains the supplementary crystallographic data for this paper. These data are provided free of charge by the joint Cambridge Crystallographic Data Centre and Fachinformationszentrum Karlsruhe Access Structures service www.ccdc.cam.ac.uk/structures.

X-ray powder diffraction

The sample was ground and filled into a Hilgenberg glass capillary (outer diameter 0.5 mm, wall thickness 0.01 mm) inside an argon filled glovebox. Due to a slight amount of adhesive oleum, a homogenous filling of the capillary was rather difficult leading to rather low intensities. The data were collected with a Bruker D8 Advance diffractometer with Cu–Kα radiation (λ = 1.54184 Å) equipped with a 1D LynxEye detector in transmission geometry. The background at lower diffraction angles is assigned to the absorption of the glass capillary.

Table 3. Crystal data and details of the structure refinements (esds in parentheses).

	$Ag[B(S_2O_7)_2]$
Temperature/K	200(2)
Molar weight/g mol^{-1}	470.92
Crystal system	monoclinic
Space group	$P2_1/c$ (no. 14)
a/pm	950.7(4)
b/pm	960.1(4)
c/pm	1173.0(4)
β/°	98.350(11)
Volume/10^6 pm^3	1059.3(7)
Z	4
Calculated density D_x/g cm^{-3}	2.953
Absorption coefficient μ/mm^{-1}	2.775
F(000)	912
Diffractometer	Bruker D8 Venture
Radiation (λ/Å)	0.71073
Absorption correction	multi-scan
Theta range/°	$2.165 < \theta < 29.996$
Index range h | k | l (min./max.)	−13/13 | −13/13 | −16/16
Reflections collected	26410
Independent reflections	3093
Observed reflections ($I > 2\sigma$)	2811
Refined parameters/Restraints	181/0
R_{int}	0.0515
R_1/wR_2 for $I > 2\sigma$	0.0213/0.0547
R_1/wR_2 for all data	0.0249/0.0557
GooF	1.072
Residual electron density (min./max.)/e$^-$ Å^{-3}	−1.292/1.209

Rietveld refinement was done using the program TOPAS V.[40] Details on the Rietveld refinement are displayed in Table S3. The background was modelled with a Chebyshev polynomial.

Temperature programmed X-ray diffraction (TPXRD) was executed within the same device using a furnace attachment. A heating ramp of 6 °C/min was applied before each measurement, the temperature was held for 15 min. The strong background between $12.5° < 2\theta < 30°$ is due to the furnace attachment.

Infrared spectroscopy

The infrared spectrum was recorded using a Bruker EQUINOX 55 FT-IR spectrometer equipped with a platinum ATR setup in a range of 4000–400 cm^{-1}.

Thermal analysis

The thermogravimetric analysis was done in an alumina crucible employing a NETZSCH STA 409 PC Luxx in nitrogen atmosphere and a heating ramp of 10 °C/min.

Acknowledgements

The authors thank the Deutsche Forschungsgemeinschaft (DFG) for financial support under the project HO 4503/5-1. Open access funding enabled and organized by Projekt DEAL.

Conflict of Interest

The authors declare no conflict of interest.

Keywords: Borosulfates · Silicate-analogues · Precious metals · Silver · Structure elucidation

[1] J. Bruns, H. A. Höppe, M. Daub, H. Hillebrecht, H. Huppertz, *Chem. Eur. J.* **2020**, *26*, 7966.
[2] H. A. Höppe, K. Kazmierczak, M. Daub, K. Förg, F. Fuchs, H. Hillebrecht, *Angew. Chem. Int. Ed.* **2012**, *51*, 6255.
[3] P. Netzsch, P. Gross, H. Takahashi, H. A. Höppe, *Inorg. Chem.* **2018**, *57*, 8530.
[4] P. Netzsch, M. Hämmer, P. Gross, H. Bariss, T. Block, L. Heletta, R. Pöttgen, J. Bruns, H. Huppertz, H. A. Höppe, *Dalton Trans.* **2019**, *48*, 4387.
[5] P. Netzsch, F. Pielnhofer, R. Glaum, H. A. Höppe, *Chem. Eur. J.* **2020**, *26*, 14745.
[6] M. Hämmer, L. Bayarjargal, H. A. Höppe, *Angew. Chem. Int. Ed.* **2020**, 10.1002/anie.202011786.
[7] M. D. Ward, B. L. Chaloux, M. D. Johannes, A. Epshteyn, *Adv. Mater.* **2020**, e2003667.
[8] L. Kahle, A. Marcolongo, N. Marzari, *Energy Environ. Sci.* **2020**, *13*, 928.
[9] S. Geller, *Science* **1967**, *157*, 310.
[10] J. N. Bradley, P. D. Greene, *Trans. Faraday Soc.* **1967**, *63*, 2516.
[11] T. Takahashi, *J. Appl. Electrochem.* **1973**, *3*, 79.
[12] J. Bruns, M. Podewitz, M. Schauperl, K. R. Liedl, O. Janka, R. Pöttgen, H. Huppertz, *Eur. J. Inorg. Chem.* **2017**, 3981.
[13] J. Bruns, M. Podewitz, K. R. Liedl, O. Janka, R. Pöttgen, H. Huppertz, *Angew. Chem. Int. Ed.* **2018**, *57*, 9548.
[14] L. C. Pasqualini, H. Huppertz, J. Bruns, *Inorganics* **2019**, *7*, 145.
[15] L. Pasqualini, O. Janka, S. Olthof, H. Huppertz, K. Liedl, R. Pöttgen, M. Podewitz, J. Bruns, *Chem. Eur. J.* **2020**.
[16] C. Logemann, D. Gunzelmann, T. Klüner, J. Senker, M. S. Wickleder, *Chem. Eur. J.* **2012**, *18*, 15495.
[17] P. J. Malinowski, M. Derzsi, A. Budzianowski, P. J. Leszczyński, B. Gaweł, Z. Mazej, W. Grochala, *Chem. Eur. J.* **2011**, *17*, 10524.
[18] L. V. Schindler, M. Struckmann, A. Becker, M. S. Wickleder, *Eur. J. Inorg. Chem.* **2017**, *2017*, 958.
[19] P. Netzsch, F. Pielnhofer, H. A. Höppe, *Inorg. Chem.* **2020**, *59*, 15180.
[20] P. Netzsch, H. A. Höppe, *Inorg. Chem.* **2020**, DOI: 10.1021/acs.inorgchem.0c02560.
[21] M. Daub, K. Kazmierczak, P. Gross, H. Höppe, H. Hillebrecht, *Inorg. Chem.* **2013**, *52*, 6011.
[22] M. Daub, H. A. Höppe, H. Hillebrecht, *Z. Anorg. Allg. Chem.* **2014**, *640*, 2914.
[23] M. Daub, H. Hillebrecht, *Eur. J. Inorg. Chem.* **2015**, *2015*, 4176.
[24] M. S. Wickleder, *Z. Anorg. Allg. Chem.* **2001**, *627*, 2112.
[25] J. Bruns, M. Eul, R. Pöttgen, M. S. Wickleder, *Angew. Chem. Int. Ed.* **2012**, *51*, 2204.
[26] P. J. Malinowski, M. Derzsi, Z. Mazej, Z. Jaglicić, B. Gaweł, W. Łasocha, W. Grochala, *Angew. Chem. Int. Ed.* **2010**, *49*, 1683.
[27] L. Pauling, *J. Am. Chem. Soc.* **1929**, *51*, 1010.
[28] L. V. Schindler, A. Becker, M. Wieckhusen, T. Klüner, M. S. Wickleder, *Angew. Chem. Int. Ed.* **2016**, *55*, 16165.
[29] T. Balić Žunić, E. Makovicky, *Acta Crystallogr. Sect. B* **1996**, *52*, 78.
[30] E. Makovicky, T. Balić-Žunić, *Acta Crystallogr. Sect. B* **1998**, *54*, 766.
[31] R. D. Shannon, *Acta Crystallogr. Sect. A* **1976**, *32*, 751.
[32] M. Jansen, *Angew. Chem. Int. Ed.* **1987**, *26*, 1098.
[33] R. Hübenthal, *MAPLE - Program for the Calculation of the Madelung Part of Lattice Energy*, Universität Gießen, **1993**.
[34] R. Hoppe, *Angew. Chem. Int. Ed.* **1970**, *9*, 25.
[35] R. Hoppe, *Angew. Chem.* **1966**, *78*, 52.
[36] K. Nakamoto, *Infrared and Raman spectra of inorganic and coordination compounds. Part A: Theory and applications in inorganic chemistry*, Wiley, Hoboken, N.J, **2009**.
[37] Bruker, *SADABS*, Bruker AXS Inc., Madison, Wisconsin, USA, **2001**.
[38] G. M. Sheldrick, *Acta Crystallogr.* **2008**, *A64*, 112.
[39] G. M. Sheldrick, *Acta Crystallogr.* **2015**, *C71*, 3.
[40] Bruker, Topas V5. General profile and structure analysis software for powder diffraction data, Karlsruhe, Germany, **2014**.

Manuscript received: December 4, 2020
Revised manuscript received: December 24, 2020
Accepted manuscript online: December 29, 2020